X-Ray Photoelectron Spectroscopy (XPS): An Introduction

David J. Morgan*

Cardiff Catalysis Institute, School of Chemistry, Cardiff University, Cardiff. CF10 3AT

XPS, photoelectron, model structure, particle size, primer, introduction

ABSTRACT: This paper serves as a primer towards X-ray photoelectron spectroscopy (XPS) and an introduction towards the information it can provide in respect of heterogeneous and nanoscale catalysis.

Introduction: The phenomenon of heterogeneous catalysis focuses on the study of reactions occurring at specific sites on typically a metal, oxidic or supported metal material. Each stage of the process is characterised by a series of basic steps beginning with surface accommodation, surface diffusion, adsorption, formation of intermediates and finally desorption of products [1]. In light of these processes, in the development of new catalysts there is a large driving force to elucidate the properties of the surface in detail; be they chemical, structural, electronic or an ensemble of these. This is especially true for changes induced by a catalytic reaction. Of course, to probe such interfaces, the technique employed must have elemental identification together with a high degree of surface sensitivity, as found in X-ray Photoelectron Spectroscopy (XPS), due to the finite depth (typically <20 nm) that the ejected analysed electrons may travel [2].

Photoemission: XPS is based upon the photoelectric effect; the phenomenon whereby a photon flux of sufficient energy, impinging on a material causes the ejection of (photo)electrons *i.e.* photoemission [2]. The kinetic energy (*EK*) of the emitted electron is measured, and the binding energy (*EB*) of the electron for a particular energy level given by the Einstein relationship: $E_K = h\upsilon - E_B$ (1), where $h\upsilon$ is the energy of the incident radiation. Typically in XPS the incident photon energy is >1200 eV, and therefore of an energy sufficient to cause electron ejection from an atoms core levels. Obtaining the spread of kinetic (*c.f.* binding) energies as a function of the photoelectron flux yields the photoelectron spectrum exhibiting all the accessible energy levels (figure 1).

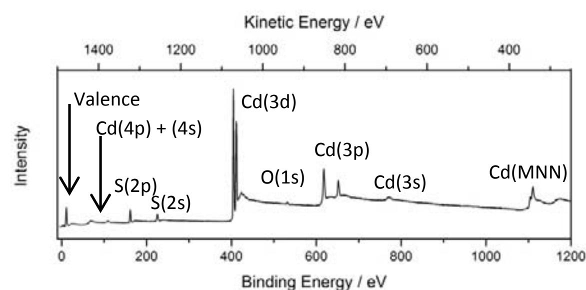

Figure 1. A typical photoelectron survey spectrum. This particular sample is cadmium sulfide (CdS).

It should be appreciated that the binding energy, *EB* is **not** equal to the orbital energy of the electron – the so-called *frozen-orbital approximation* [3] – as the energy levels in the ionised species relax to shield the newly formed core-hole, and thus the observed value of *EB* is larger than that predicted by Koopmans' theorem.

Therefore, a more useful expression for *EB* is: $E_B = E_i - E_f$ (2), where *Ei* and *Ef* are the total energies of the initial (ground) and final (ionised) states respectively. By combining equations (1) and (2), it is evident that anything which affects the initial or final state of the emitting atom will have an effect on the binding energy.

Final State Effects: To minimise the increased energy, electrons in the ionised species undergo reorganisation resulting in a number of possible final states, each with their own corresponding energy and therefore extra peaks appear in the photoelectron spectrum.

Shake-up occurs when an electron within the emitting atom is promoted to a higher level during the photoionisation process, thus the kinetic energy of ejected electron is reduced by the amount of energy required for the transition and therefore the main photoelectron peak is accompanied by a satellite peak at an apparently higher binding energy. Whilst these features are not overly common in XPS spectra, perhaps the most notable exceptions are the 2p spectra of first-row d-band metals, and the pi-pi* transition (i.e. bonding to antibonding transition) in the C(1s) spectra of aromatic organic compounds.

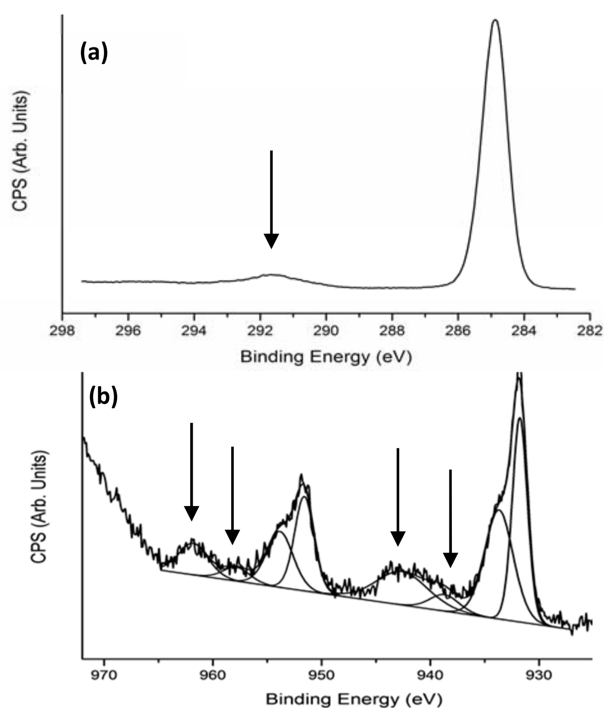

Figure 2. Shake-up satellites for (a) Aromatic-based compounds and (b) Cu(II) species in a Cu(0)/Cu(II) mixed state catalyst. The arrows indicate the satellite structure

Some materials, especially lanthanoid (*e.g.* lanthanum, cerium and europium) compounds for example [4] also exhibit *shake-down* peaks, where the satellites appear at lower binding energy due to an apparent energy gain [5]; the reader is directed to the given references for further discussion. *Multiplet splitting* arises from the coupling of the remaining unpaired electron spin with unpaired spins in the valence levels of an atom, again leading to satellite peaks in the photoelectron spectrum. All transition metals with unfilled *p* and *d* orbitals, as well as the rare-earth materials with unfilled *f* orbitals all exhibit this phenomenon [6].

Whilst the nature of the aforementioned phenomena is dependent upon the electronic structure of the initial or final states, for all orbitals where the angular momentum quantum number (l) > 0 (i.e. *p*, *d* and *f* levels) *spin-orbit splitting* is always observed. Here coupling will occur between the fields of spin (s) and the angular momentum (l), resulting in a total angular momentum given by $j=|l+s|$, or more conveniently expressed as $j=(l \pm ½)$, with the multiplicities proportional to $(2j+1)$. This is shown in figure 3.

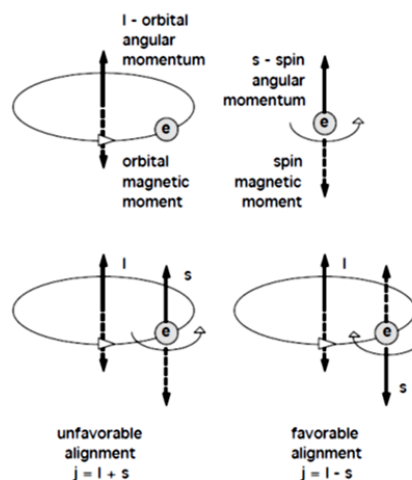

Figure 3. The coupling leading to spin-orbit splitting

For example, the Ti(2p) level, j has the values of $^3/_2$ and $^1/_2$ and thus two peaks are observed in the spectrum; specifically Ti(2p$_{3/2}$) and Ti(2p$_{1/2}$), the ratio of intensities in this case is 2:1. Similarly for Rh(3d), the j values are $^5/_2$ and $^3/_2$ yielding two peaks, with an intensity ratio of 3:2 (figure 4).

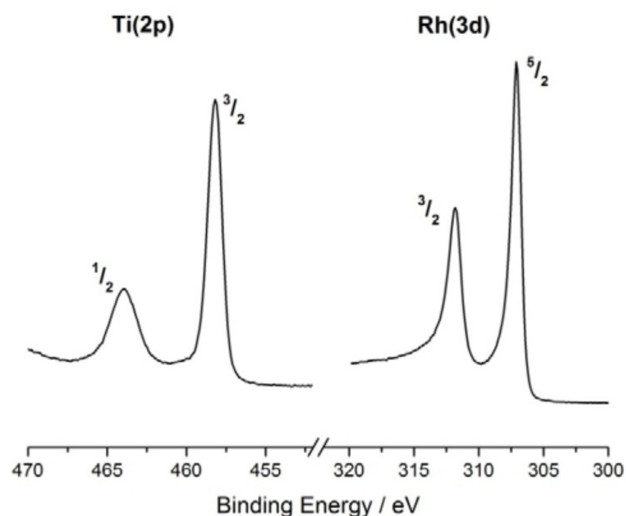

Figure 4. Spin-orbit splitting for (a) Ti(2p) in TiO_2 and (b) Rh(3d) for metal foil

Core-Hole Neutralisation: Photoemission results in the formation of a *core hole*; however core-holes undergo rapid neutralisation by electrons from higher levels resulting in a quantum of energy which is released in one of two ways: (a) *Fluorescence*, or (b) *Auger Emission*; the probability of which will dominate being dependent on the atomic number (Z) of an element. Auger peaks, like photoelectron peaks, are observed in the photoelectron spectrum (see for example the Cd(MNN) peak in figure 1) and can be used to aid identification of species and oxidation state where the core levels may not be overly sensitive to a change in oxidation state (for example Zn); we return to this later.

The formation of the *core-hole* generates a charge on the surface and consequently the ejected photoelectrons must also overcome this charged layer resulting in a decreased kinetic energy (hence higher binding energy). Typically this is not a problem for conductive samples whereby they are grounded *via* the spectrometer, however semiconducting and insulating samples rapidly achieve a positive potential on the surface. To circumvent this accumulation, particularly for monochromatic X-ray sources, the use of a *charge neutraliser* (sometimes called a *charge compensator*) is used, which delivers a flux of low energy electrons at the surface and "moving" the photoelectron peaks to lower energies and such methods are typically used for the study of heterogeneous catalysts and biological specimens where the samples are inherently insulating. During subsequent spectral analysis this shift in energy must be accounted for and an internal reference is used; typically the C(1s) signal from adventitious carbon present on *all* surfaces and typically assigned a value of 284.7 eV for catalysts, or 285 eV for organic networks such as polymers [7], although other references may be used (*e.g.* Si(2p) in SiO_2 [8]). For achromatic sources, the high levels of Bremsstrahlung radiation can aid in charge neutralisation, although an internal reference is still required. Types of X-ray sources employed in XPS are covered in the following section.

Instrumentation: XPS instrumentation is common place in many materials, physics or chemistry laboratories across the world and is one of the main techniques used to probe surfaces in industry; for example semiconductor manufacturing [9]. The spectrometer itself is of stainless steel construct and equipped with a combination of pumps to obtain ultra-high vacuum (UHV) conditions of typically *ca*. 10^{-10} mbar. Standard laboratory X-ray sources are all of similar design whereby X-ray photons are generated by means of electron bombardment of a metal anode target (typically aluminium ($h\upsilon$ = 1486.6 eV) or magnesium ($h\upsilon$ = 1253.6 eV)) which is held at a high potential (typically 15 kV), and which results in primarily the emission of the $K_{1,2}$ radiation line. Typically spectrometers will have a switchable Al/Mg dual anode source which is useful to distinguish between photoemission and Auger peaks since the kinetic energy of the latter is independent of $h\upsilon$. Most modern instruments offer monochromatic sources (again typically aluminium, although silver is rapidly becoming a popular choice [10; 11]; typical advantages of monochromatic sources are reduction of the inherent linewidth of the exciting radiation, removal of secondary x-ray emission lines (for example the $K\alpha_{3,4}$ line) and therefore overall improved resolution.

Detection of photoelectrons is achieved typically through an electrostatic concentric hemispherical analyser (CHA) and is perhaps the most commonly encountered in modern spectrometers. Typically for analysis the photoelectrons are retarded at the analyser entrance to the *pass energy* (PE) in order to enhance the resolution of the photoelectrons; this is common place and referred to the constant analyser energy (CAE) mode of operation whereby the energy resolution is independent on the analyser transmission [12]. Detection of the electrons is achieved through use of a bank of channeltron electron multipliers or a channel plate array. The interested reader is directed to [12] and references therein, for a detailed explanation of the instrumentation employed for electron spectroscopy.

Aspects of XPS

Why is XPS Surface Sensitive? Whilst X-rays penetrate deeply in to a sample, the generated photoelectrons undergo a high degree of scattering within the bulk of the solid; therefore only those electrons originating in the near surface region escape with no energy loss. This depth may be quantitatively defined by the parameter λ, termed the *inelastic mean-free path* (IMFP) of the photoelectron and is generally defined as the distance an electron travels with a probability $1/e$ of *not* undergoing inelastic scattering.

Values for λ are typically in the range of 1-3 nm and since 95% of photoelectron intensity comes from a depth of approximately 3λ [2], yields an information depth of approximately 10 nm (figure 5). λ is dependent on the kinetic energy of the electron as well as the solids composition. For kinetic energies greater than 100 eV, λ increases with kinetic energy according to $\lambda \propto E_k^n$ where n = 0.5 – 0.75, depending on the characteristics of the analyser.

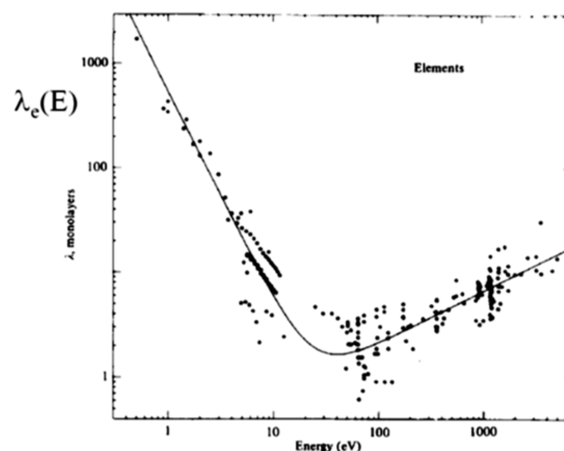

Figure 5. The dependence of λ on kinetic energy [1]

The Chemical Shift (an Initial State Effect) and the Auger Parameter: XPS can provide information on the environment of atoms through the so-called *chemical shift*. Consider the binding energy of an emitted photoelectron, the energy depends on the localised charge of the emitting atom, which itself is determined by the ligands to which it is bound. This is termed an *initial state effect*, since the electron energies are perturbed before photoionisation. Figure 6 shows a two simple cases of this, whereby in the first example, the polymer Ethyl trifluoroacetate has increasing energy C(1s) peaks corresponding to the increasing positive charge on the carbon atoms due to the substituent's electronegativity. In the second example we see the same effect due to the charge on the sulfur atoms in two different states; atomic sulfur and sulphate.

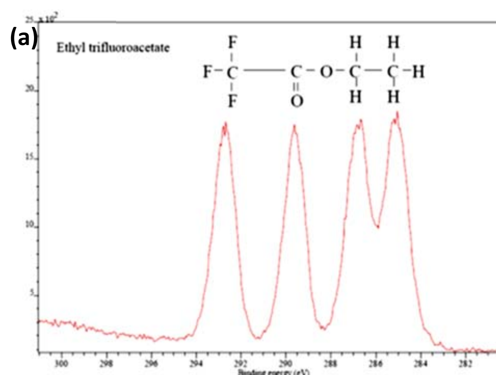

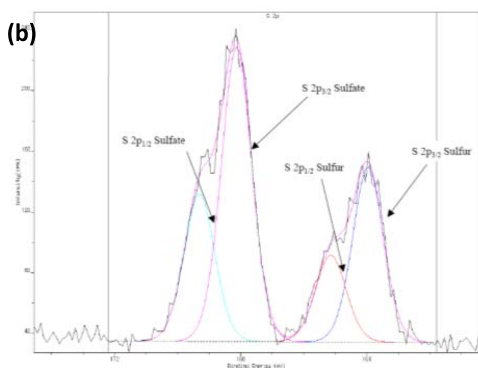

Figure 6. The chemical shift for (a) ethyl trifluoroacetate and (b) sulfur vs. sulfate

As touched upon earlier, for some metals (*e.g.* zinc) oxidation does not lead to measureable chemical shifts due to the counteracting investigate the Auger peaks since Auger transitions involving valence electrons invariably exhibit larger chemical shifts than those observed for the photoemission peaks. In light of this, much use has been made of the *Auger parameter* (α). Defined as $\alpha = E_B + E_k$ (3), where E_B and E_k are the binding and kinetic energies of the main photoemission and Auger peaks [13]. From studies of compounds for a particular element (*e.g.* Cu, CuO, CuCl, $CuCl_2$ *etc*) and plotting the kinetic energies of the Auger electron and the binding energies of photoelectrons on orthogonal axes (figure 7), chemical state plots may be derived which are useful in distinguishing related compounds [13].

An inherent advantage of the Auger parameter is its insensitivity to charging, meaning it can be applied equally to all systems, as well as being independent on the incident photon energy. For some instances where the Auger peak is not readily apparent, the use of bremsstrahlung radiation from a conventional achromatic X-ray source may be used to probe these transitions and include the Al, Si, C and S *KLL* Auger lines [14].

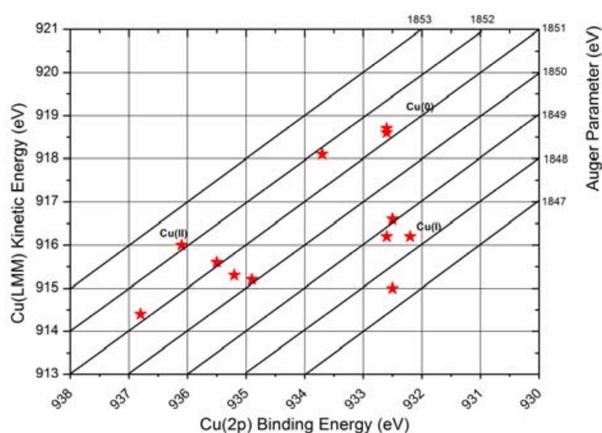

Figure 7. Example of a (Wagner) chemical state plot for copper compounds. For clarity the actual values and compounds have been omitted

Quantification: The intensities of core-level peaks may be used to estimate the elemental composition of a solid through either a first-principles approach or via relative sensitivity factors (RSFs).

In first principles studies, the integrated area of a photoelectron peak is proportional to the concentration of that element in the analysed area. The signal I_x from element x is given by: $I_x = Anf\mu_x\lambda\theta T$ (4), where A is the area if the analyte, n = number of atoms cm^{-3} of the analyte, f is the X-ray flux in photons $cm^{-2}.s$, μ = photoionisation cross-section for a particular emitting orbital of element x (which have been by tabulated by Scofield [15]), θ = angular factor for the instrument, λ = IMFP, and T is the transmission function of the analyser (electron detection efficiency).

Under a given operating mode, the analysed area, x-ray flux and any other instrumental factors remain constant, and we can simplify the equation to: $I_x \propto \mu_x n\lambda$ (5).

This relationship is applied to two peaks from different elements, making use of the fact that for a given material the ratio of IMFPs depends only on the kinetic energies of the electrons. The latter RSF method is based on measurements made on a range of standard compounds [16] and therefore ultimately incorporate the terms μ and λ.

Environmental and Beam Effects: An often neglected phenomena in XPS is the effect of beam damage. Whilst this is perhaps more widely considered in the analysis of polymers [7; 17], the same is true for many systems containing particulate metals; especially those containing Cu(II), Au(I), Au(III) and Pd(II) species. It is clear for catalytic studies, that if reduction of these species occurs during the analysis, any deductions made on (for example) the active species of a catalyst may arise as a result of incorrect analysis. It is well known that the unstable oxide Au_2O_3 reduces under X-ray analysis to yield metallic Au with the evolution of oxygen [18]. However the same appreciation is not always given to the cationic gold species present in catalysts; for example figure 8 shows the reduction of cationic Au(III) to metallic gold for a 5wt% dried Au/CeO_2 catalyst during an analysis time of 10 minutes. Similarly the reduction of Cu(II) species [19] is widely known, but again it is not always apparent if experimentalists actively check for this in XPS analysis. Therefore it is good experimental practice to acquire data for such regions at least twice – typically at the start and end of the analysis run in order to elucidate any reduction.

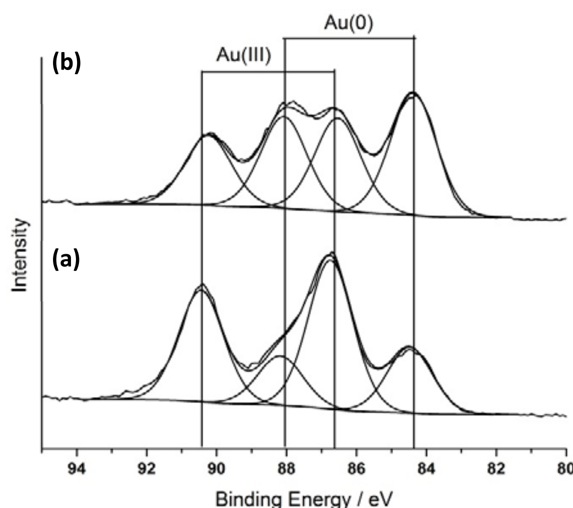

Figure 8. The X-ray induced reduction of Au(III) to Au(0).
(a) Fresh Catalyst, (b) after 10 min X-ray exposure during analysis

Particle Size Determination: Without access to the latest generation TEM microscopes [20], the size of particles and nature of the support of catalyst samples make direct observation difficult, especially for particles of diameter ~ <3 nm. XPS, through its pronounced surface sensitivity may be used for estimation of particle sizes, and different methods have been put forward with success [21-24].

To obtain particle size information from XPS, the photoelectron signals must be modelled appropriately. The methods of Kerkhof and Moulijn [21] and Davis [22] use a model whereby the ratio of signals from particles to that of the support with a model, typically layered structure and has been shown to be successful in many cases; however the inherent problem with such models is the reliance on crystalline uniformity and homogenous nature of the surface. A second approach uses the signal intensity ratio of photoelectron or Auger-electron peaks of different kinetic energies arising from the particles. In the work of Yang and Sacher [23; 24] they have used this method for supported Cu clusters and found excellent agreement between the XPS (average) derived values for cluster size and those determined by TEM; this was achieved by measuring a peak intensity ratio and applying the following equation:

$\frac{I_1}{I_2} = \frac{I_1^0\left[1-\exp\left(-d/\lambda_1\right)\right]}{I_2^0\left[1-\exp\left(-d/\lambda_2\right)\right]}$ (6), where I_1^0 and I_2^0 are the intensities of the two peaks that would be obtained from infinitely thick layers (*i.e.* $d >> \lambda$) under identical analysis conditions. This ratio would be equal to the ratio of appropriately determined sensitivity factors; d is the average cluster diameter and λ_n refers to the appropriate IMFPs for the kinetic energies of the two measured transitions.

Of course contamination can alter peak ratios and will ultimately limit any accuracy these methods may have, however assuming that any carbon contamination is uniform the methods of Evans [25] or Mohai [26] to account for overlayer correction may be applied to improve accuracy.

Nanostructures, peak energies and background analysis: It is well known that nanoparticles and metal clusters, when supported on, for example oxide, sulfide or carbon supports, exhibit binding energies that differ from those of the bulk material by up to *ca.* 0.6 eV [27; 28]. The nature of these shifts is sometimes so regular that it has been proposed that the binding energy may be used as a pointer towards particle size. However, this may be a simplistic view as several other causes of binding energy shifts have been found to come from size, strain, the charge due to lattice-substrate interactions and final-state relaxation effects. Regardless of this, the photoelectron peak shifts, when combined with Auger line shifts to determine the Auger parameter, correlations can be made between the variation of the Auger parameter and the binding energy shifts with particle size and the turn over frequency (TOF) of catalysts.

The atomic distribution of elements within a sample will not only affect the relative peak intensities, but will also affect the inelastic scattered electrons which add to the continuous, step-like background observed in XPS spectra (see figure 1 for example). Work pioneered by Tougaard [29; 30] involves a systematic approach to using this inelastic background to obtain elemental distribution information in the outer 20 nm of a sample. Figure 9 illustrates four different elemental distributions of Cu in a lattice. Whilst the Cu(2p) intensity is identical, the lower kinetic energy 'tail' are significantly different due to the degree of scattering.

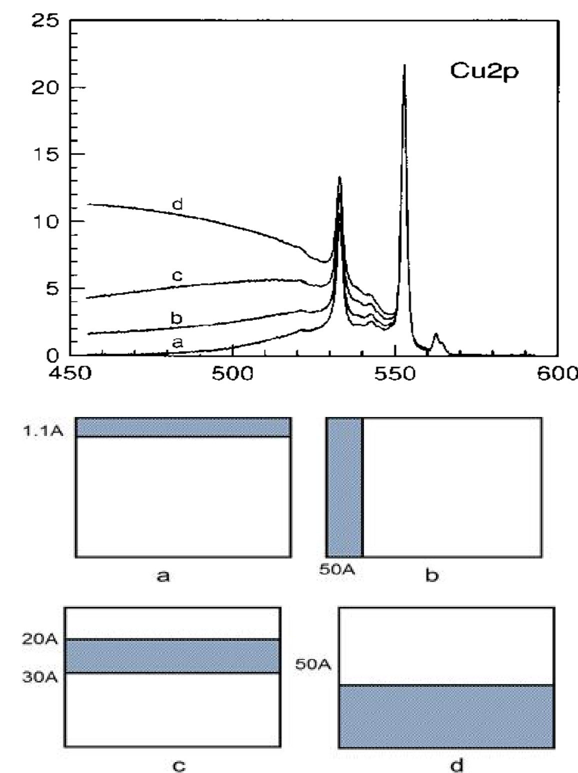

Figure 9. Cu(2p) spectra for four different depth distributions of copper. Note how the four distributions yield the same Cu(2p) intensity, but have increasingly different backgrounds. Adapted from [29].

Using this information can yield valuable information about elemental segregation towards the surface during calcination or the reverse situation; incorporation in to the bulk.

Layered Structures: By far, most materials examined will have a change in composition as a function of depth; therefore knowledge of the elemental concentrations within the interfacial region is of importance. To investigate this in a conventional laboratory, two methods are typically employed: (a) *Sputter-Depth Profiling* and (b) *Angle-Resolved XPS (ARXPS).*

(a) Sputter-Depth Profiling: In this method of profiling, the sample of interest is bombarded with a flux of inert gas ions (typically argon) generated by an ion-gun. The collision of the ions with the surface removes clusters of atoms from the surface, thereby sputtering the sample in a layer-by-layer like fashion. By performing XPS analysis after each sputtering cycle, the concentration gradient can be calculated. However, the one pitfall of this method is *"preferential sputtering"*, whereby the effects of the sputtering process can preferentially remove one element over another and therefore the changes do not represent the original concentration profile, an example of this is the sputtering of TiO_2 which leads to the preferential removal of oxygen (the lighter mass elements are typically preferentially removed), resulting in a series of reduced titania states which do not reflect the true depth-profile.

(b) Angle-Resolved XPS (ARXPS): XPS supplies information in a range typically no greater than *ca.* 10 nm, this range can be minimised by rotation of a sample with respect to the entrance of the electron analyser. The relationship between the IMFP and the average photoelectron escape depth is given by: $d = \lambda \cos \phi$ (7), where d = depth of the photoelectron escape and ϕ the *take-off angle* (angle between the flight of the photoelectrons from the solid and the surface itself). Figure 10 shows two possible paths for the ejection of the photoelectron (AB and AC respectively). The path length along AB is d, and along AC equal to $d\cos\phi$; where ϕ is the angle between AC and the surface normal. Since AC>AB the probability of inelastic scattering along AC is greater than along AB, and so the electrons along AB are detected with negligible energy loss. Therefore, by increasing ϕ through rotating the sample with respect to the analyser entrance an enhancement in surface sensitivity is achieved.

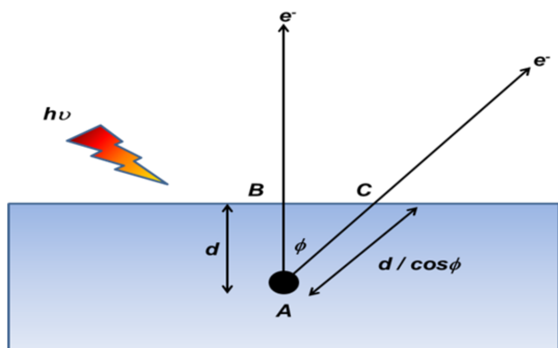

Figure 10. Typical ARXPS geometry

Through collection of photoelectron spectra at a series of angles, the data can be analysed to generate concentration profiles. The interested reader is directed to the work of Paynter [31] and references therein for further discussion.

Thickness Determination: Layered structures are of great importance in industry as well as catalysis. For example, semiconductor based devices are typically made of layered materials and the performance of these devices is related to the thickness of each layer. Whilst this is not a true catalytical based example, catalyst materials may themselves be layered (*e.g.* core-shell particles or mixed-oxide systems), or "surface science" models of catalytic systems may be formed in a layer-by-layer fashion in order to elucidate active sites; see for example [32].

To illustrate such analysis we will consider the simplified system of an Al_2O_3 layer on a clean Al foil, or SiO_2 on a Si wafer (figure 11); where in both cases the kinetic energies and IMFP's are very similar for the oxide and elemental peaks.

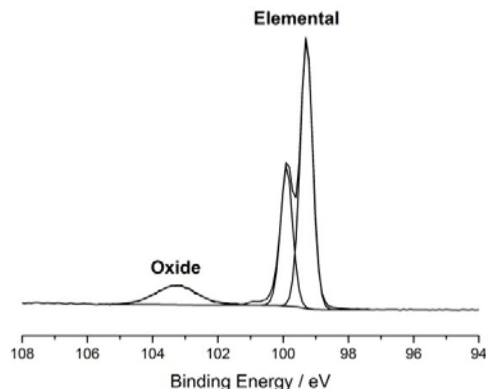

Figure 11. Native SiO_2 layer on a high purity Si wafer. The oxide thickness has been determined to be *ca* 0.7 nm by the method presented in [33].

Carlson [33; 34] and Strohmeier [35] both showed for a metal with an oxide overlayer on it (not this layer is considered to be uniform), the relative intensities of the metal (I_M) and the oxide (I_O) photoelectron peaks is given by: $\frac{I_M}{I_O} = \frac{N_M \lambda_M}{N_O \lambda_O} \frac{\exp\left[\left(-d/_{\lambda_O \sin\theta}\right)\right]}{1-\exp\left[\left(-d/_{\lambda_O \sin\theta}\right)\right]}$ (8), where N_x = volume densities of the metal atoms in the metal or oxide, l_x = the IMFP of the appropriate photoelectrons, d = oxide thickness (Å) and q = electron take-off angle. Rearrangement therefore gives: $d = \lambda_O \sin\theta \ln\left[\frac{N_M \lambda_M}{N_O \lambda_O} \frac{I_O}{I_M} + 1\right]$ (9). Note that equation (9) does not take in to account any surface contamination (*e.g.* carbon overlayer), however for aluminium this is typically 10-20 Å and can be accounted for within the analysis (see references in section 3.4).

More recently, Cumpson has developed the "thickogram" to measure overlayer thickness [36]. A graphical method, especially suited for samples where the overlayer has a different elemental chemistry than the substrate (*e.g.* Yttrium on Silicon), the method is advantageous for several reasons, specifically: the adventitious carbon surface contamination is unimportant, cancellation of any instrumental factors, method is applicable to a wide range of kinetic energies and valid for a wide range of film thicknesses. The accuracy of this method has been shown to be approximately ±10%, based on the calculated attenuation lengths, such as those published through NIST [37]. The usefulness of the "thickogram" was enhanced by Shard *et al.* who introduced "topofactors" to allow the method to be applied to non-planar surfaces, such as spheres and cylindrical geometries [38]

Concluding Remarks: This paper has sought to serve as a primer and to introduce the reader to the strength and application of XPS in catalytic and nanoscale analysis and the considerations that should be given therein.

AUTHOR INFORMATION

Corresponding Author

* MorganDJ3@cardiff.ac.uk

Funding Sources

The author greatly acknowledges the EPSRC for funding through the access to materials research equipment scheme (EP/F019823/1) and colleagues and mentors for helpful advice

REFERENCES

[1] G.A. Somorjai, Y. Li, Introduction to Surface Chemistry and Catalysis, Second Edition, John Wiley & Sons, 2010.

[2] S. Hufner, Photoelectron Spectroscopy Principles and Applications, Springer, 2003.

[3] T. Koopmans, Physica 1 (1934) 104-113.

[4] E. Bêche, P. Charvin, D. Perarnau, S. Abanades, G. Flamant, Surface and Interface Analysis 40 (2008) 264-267.

[5] A. Kotani, T. Jo, J.C. Parlebas, Advances in Physics 37 (1988) 37-85.

[6] J. Moulder, W. Stickle, P. Sobol, K. Bomben, Handbook of X-ray Photoelectron Spectroscopy, Perkin-Elmer Corp, Eden Prairie, 1992.

[7] G. Beamson, D. Briggs, High resolution XPS of organic polymers, Wiley, 1992.

[8] M.J. Remy, M.J. Genet, G. Poncelet, P.F. Lardinois, P.P. Notte, Journal of Physical Chemistry 96 (1992) 2614-2617.

[9] C.R. Brundle, G. Conti, P. Mack, Journal of Electron Spectroscopy and Related Phenomena 178 (2010) 433-448.

[10] R. Paynter, M. Edgell, J. Castle, Journal of Electron Spectroscopy and Related Phenomena 40 (1986) 1-9.

[11] http://surface.kratos.com/Monochromatic-Ag-x-ray-Source/monochromated-ag-x-ray-source.html. (last accessed 22/11/11)

[12] Surface Analysis by Auger and X-ray Photoelectron Spectroscopy, IM Publications, 2003.

[13] C.D. Wagner, A. Joshi, Journal of Electron Spectroscopy and Related Phenomena 47 (1988) 283-313.

[14] J. Watts, J. Wolstenholme, An introduction to surface analysis by XPS and AES, Wiley, 2003.

[15] J. Scofield, Journal of Electron Spectroscopy and Related Phenomena 8 (1976) 129-137.

[16] Practical Surface Analysis - Auger and X-ray Photoelectron Spectroscopy Wiley Interscience, 1990.

[17] D. Briggs, Surface analysis of polymers by XPS and static SIMS, Cambridge University Press, Cambridge, UK, 1998.

[18] H. Tsai, E. Hu, K. Perng, M. Chen, J.-C. Wu, Y.-S. Chang, Surface Science 537 (2003) L447-L450.

[19] V. Di Castro, G. Piredda, Chemical Physics Letters 114 (1985) 109-113.

[20] A.A. Herzing, C.J. Kiely, A.F. Carley, P. Landon, G.J. Hutchings, Science 321 (2008) 1331-5.

[21] F.P.J.M. Kerkhof, J.A. Moulijn, The Journal of Physical Chemistry 83 (1979) 1612-1619.

[22] S. Davis, Journal of Catalysis 117 (1989) 432-446.

[23] D.Q. Yang, E. Sacher, Surface Science 516 (2002) 43-55.

[24] D.Q. Yang, M. Meunier, E. Sacher, Applied Surface Science 173 (2001) 134-139.

[25] S. Evans, Surface and Interface Analysis (1998).

[26] M. Mohai, I. Bertóti, in: H.J. Mathieu, B. Reihl, D. Briggs (Eds.), ECASIA 95, John Wiley & Sons, Chichester, 1996, pp. 675-678.

[27] M.G. Mason, Physical Review B 27 (1983) 748-762.

[28] G.K. Wertheim, S.B. DiCenzo, Phys Rev B Condens Matter 37 (1988) 844-847.

[29] S. Tougaard, Surface and Interface Analysis 26 (1998) 249-269.

[30] S. Tougaard, Journal of Vacuum Science & Technology A: Vacuum, Surfaces, and Films 14 (1996) 1415.

[31] R.W. Paynter, Journal of Electron Spectroscopy and Related Phenomena 169 (2009) 1-9.

[32] N. Khan, A. Uhl, S. Shaikhutdinov, H. Freund, Surface Science 600 (2006) 1849-1853.

[33] T.A. Carlson, Surface and Interface Analysis 4 (1982) 125-134.

[34] T. Carlson, G.E. McGuire, Journal of Electron Spectroscopy and Related Phenomena 1 (1973) 161-168.

[35] B.R. Strohmeier, Surface and Interface Analysis 15 (1990) 51-56.

[36] P.J. Cumpson, Surface and Interface Analysis 29 (2000) 403-406.

[37] C.J. Powell, A. Jablonski, NIST Electron Effective-Attenuation-Length Database - Version 1.3, National Institute of Standards and Technology, Gaithersburg, MD, 2011.

[38] A.G. Shard, J. Wang, S.J. Spencer, Surface and Interface Analysis 41 (2009) 541-548.

.